

## Effect of Preparation Method on the Activity of Fe<sub>2</sub>O<sub>3</sub>-NiO/γ-Al<sub>2</sub>O<sub>3</sub> Catalyst in Decomposition of Methane

G. Yergaziyeva<sup>1,2\*</sup>, N. Makayeva<sup>1,2</sup>, M. Anissova<sup>1</sup>, K. Dossumov<sup>1</sup>, M. Mambetova<sup>1</sup>, Z. Shaimerden<sup>2</sup>, A. Niyazbaeva<sup>2</sup>, E. Akkazin<sup>2</sup>

<sup>1</sup>Institute of Combustion Problems, 172, Bogenbai batyr str., Almaty, Kazakhstan

<sup>2</sup>al-Farabi Kazakh National University, 71, al-Farabi ave., Almaty, Kazakhstan

### Article info

Received:  
14 April 2022

Received in revised form:  
10 May 2022

Accepted:  
24 June 2022

### Keywords:

Decomposition  
Methane  
Catalyst  
Hydrogen  
Graphene-like carbon

### Abstract

The effect of method preparation on the activity of Fe<sub>2</sub>O<sub>3</sub>-NiO/γ-Al<sub>2</sub>O<sub>3</sub> catalyst was investigated in process decomposition of methane. Fe<sub>2</sub>O<sub>3</sub>-NiO/γ-Al<sub>2</sub>O<sub>3</sub> catalyst was prepared by impregnation and solution combustion methods. The samples were characterized by X-ray phase analysis (XRD), temperature-programmed hydrogen reduction (TPR-H<sub>2</sub>), BET and Raman spectroscopy. It has been shown that the method of preparation plays an important role in regulating the textural and morphological properties of catalysts and provides a difference in their catalytic activity. The synthesis of the Fe<sub>2</sub>O<sub>3</sub>-NiO/γ-Al<sub>2</sub>O<sub>3</sub> catalyst by the solution combustion method, in comparison with the capillary impregnation method, leads to the formation of a large amount of FeNi and FeAl<sub>2</sub>O<sub>4</sub> solid solutions, which ensured good catalytic activity at high temperatures. The Fe<sub>2</sub>O<sub>3</sub>-NiO/γ-Al<sub>2</sub>O<sub>3</sub> catalyst synthesized by the solution combustion method demonstrated good activity with a hydrogen yield of 52% within 150 min of the reaction without any deactivation. According to the results of Raman spectroscopy, graphene-like carbon was obtained on the surface of the catalysts. On the catalyst of Fe<sub>2</sub>O<sub>3</sub>-NiO/γ-Al<sub>2</sub>O<sub>3</sub> (CI) synthesized by capillary impregnation, 4–5 layer graphene on Fe<sub>2</sub>O<sub>3</sub>-NiO/γ-Al<sub>2</sub>O<sub>3</sub> (SC)-6-7 layer graphene is formed.

## 1. Introduction

The catalytic decomposition of methane (CDM) is a promising method for obtaining pure hydrogen without CO<sub>x</sub>. The advantage of catalytic decomposition of methane to hydrogen in comparison with steam methane reforming, water electrolysis, and other processes are described in detail in [1–3]. Nickel oxide is widely studied as catalysts for CDM, but the main disadvantage of these catalysts is its rapid deactivation. Iron oxide is a promising catalyst that is not inferior in activity to nickel catalysts. Iron, like nickel, has partially filled 3d orbitals to facilitate the dissociation of hydrocarbons due to the partial acceptance of electrons [4].

Recently, monometallic Fe catalysts deposited on oxide supports, Al<sub>2</sub>O<sub>3</sub> and SiO<sub>2</sub>, have been widely studied [5–7].

Murata et al. [5] compared the activity of 10 wt.% Fe/Al<sub>2</sub>O<sub>3</sub> and 10 wt.% Fe/SiO<sub>2</sub> catalysts in methane decomposition under the same conditions. The authors found that the methane conversion was higher on the 10 wt.% Fe/Al<sub>2</sub>O<sub>3</sub> catalyst and amounted to 75%, while the methane conversion on 10 wt.% Fe/SiO<sub>2</sub> was only 10%. The authors of [6] also conducted comparative studies of the activity of 20 wt.% Fe/Al<sub>2</sub>O<sub>3</sub> and 20 wt.% Fe/SiO<sub>2</sub> in the decomposition of methane under the same conditions. The results showed that at a reaction temperature of 700 °C, a catalyst of 20 wt.% Fe/SiO<sub>2</sub> provides 5% methane conversion, while 20 wt.% Fe/Al<sub>2</sub>O<sub>3</sub>, the conversion of methane was 83%. The authors explain the low activity of the iron catalyst supported on silicon oxide compared to aluminum oxide with the low specific surface area and pore volume of the 20 wt.% Fe/SiO<sub>2</sub> catalyst.

The authors of [8–10] reported on the promoter effect of some transition metal additives on the characteristics of iron-containing samples in the

\*Corresponding author.

E-mail addresses: [ergaziyeva\\_g@mail.ru](mailto:ergaziyeva_g@mail.ru)

decomposition of methane. The authors of [8] studied the activity of Fe/Mo/MgO (respectively, the molar ratio is 50:7.5:42.5) in the decomposition of methane, at 900 °C the conversion of methane was 87%. The authors reported that the combination of Fe particles with Mo will help prevent the agglomeration of Fe particles under operating conditions at temperatures above 800 °C, which positively affects its activity. Pudukudi et al. [11] studied the activity of the 25 wt.% Fe/25 wt.% Co/SBA-15 catalyst in the decomposition of methane at 700 °C. The catalyst was highly active due to the formation of bimetallic alloys between iron oxide and cobalt, the hydrogen yield was 51%.

From the analysis of the literature, it follows that the activity of iron oxide is affected by both the nature of the carrier and the modifying additives. Iron-containing catalysts supported on alumina are more active compared to catalysts supported on silicon oxide due to effective textural characteristics. Bimetallic iron catalysts are active compared to monometallic ones due to the formation of alloys between the iron oxide and the promoter.

It is known [12, 13] that the catalyst synthesis method plays an important role in the formation of the active phase, porous structure, etc. Therefore, it was interesting to study the effect of the synthesis method on the activity and physicochemical characteristics of bimetallic iron-containing catalysts. The purpose of this work is to study the effect of preparation methods (capillary impregnation and solution combustion) on the activity of the  $\text{Fe}_2\text{O}_3\text{-NiO}/\gamma\text{-Al}_2\text{O}_3$  catalyst in the decomposition of methane to hydrogen and to study the physicochemical properties of the catalysts.

The choice of the synthesis method as capillary impregnation and combustion of the solution is justified by the fact that these methods have a number of advantages compared to other methods (sol-gel, deep impregnation, etc.): relative simplicity, less harmful waste and more efficient use of a low-percentage active component, there is no loss of the impregnating solution, which is especially important in the manufacture of expensive catalysts [14].

## 2. Experimental

$\text{Fe}_2\text{O}_3\text{-NiO}/\gamma\text{-Al}_2\text{O}_3$  catalysts (Fe:Ni oxide ratio = 3:1) were prepared by capillary impregnation of support ( $\gamma\text{-Al}_2\text{O}_3$ , Changhai Jiuzhou Chemicals Co.) according to its moisture capacity aqueous solutions of salts  $\text{Ni}(\text{NO}_3)_2 \cdot 6\text{H}_2\text{O}$  (SUST: 4055-70) and  $\text{Fe}(\text{NO}_3)_3 \cdot 9\text{H}_2\text{O}$  (SUST: 4111-74) and the

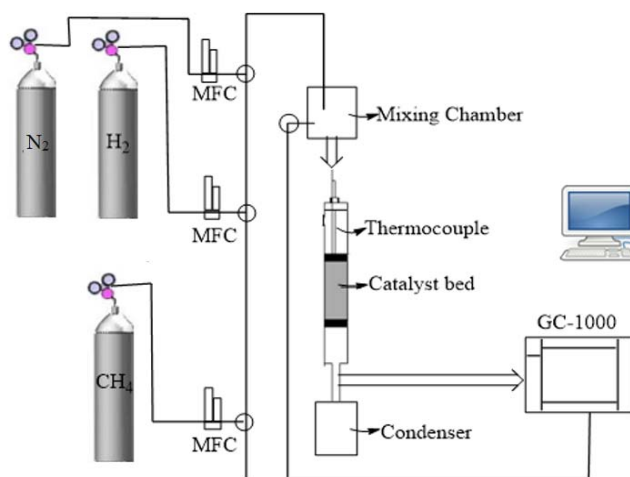


Fig. 1. Scheme of a flow-through installation.

solution combustion method with the addition of a dispersing agent (urea). Catalysts synthesized by capillary impregnation of  $\text{Fe}_2\text{O}_3\text{-NiO}/\gamma\text{-Al}_2\text{O}_3$  (CI) and combustion in a solution of  $\text{Fe}_2\text{O}_3\text{-NiO}/\gamma\text{-Al}_2\text{O}_3$  (SC) were dried at 300 °C (2 h) and calcined at 500 °C for 3 h.

Testing the activity of  $\text{Fe}_2\text{O}_3\text{-NiO}/\gamma\text{-Al}_2\text{O}_3$  (CI) and  $\text{Fe}_2\text{O}_3\text{-NiO}/\gamma\text{-Al}_2\text{O}_3$  (SC) catalysts in methane decomposition were carried out in a flow laboratory setup (Scheme 1).

The decomposition of methane was carried out in a quartz flow reactor (length 36 cm, inner diameter 1 cm). For each run 2 ml of fresh catalyst previously reduced with 6% H<sub>2</sub>/94% N<sub>2</sub> at 750 °C for 3 h was used. After reduction, hydrogen was removed by a nitrogen flow from the reaction system, then a methane/nitrogen mixture was supplied at a given temperature at a flow rate of 160 ml/min, the methane content in the initial reaction mixture was 6 vol.%. Process conditions: reaction temperature  $T = 650\text{--}850$  °C, gas volumetric flow rate (methane:nitrogen)  $\text{WHSV} = 5000$  h<sup>-1</sup>, atmospheric pressure.

The reaction products were analyzed on a Khromos GH-1000 chromatograph (Russia). Two columns were used to analyze possible reaction products: a packed column ( $l = 1$  m,  $d = 2$  mm) with CaA sorbent for hydrogen analysis; an HP/Plot Q column was used to identify CH<sub>4</sub>, CO<sub>2</sub> and CO. The first analysis of the reaction products was carried out 15 min after methane was passed through the catalyst. The efficiency of the catalysts was expressed in terms of methane conversion and hydrogen yield.

Methane conversion and hydrogen yield were calculated according to the following Eqs. (1) and (2):

$$CH_4 \text{ conversion (\%)} = \frac{CH_{4in} - CH_{4out}}{CH_{4in}} \times 100\% \quad (1)$$

$$H_2 \text{ Yield (\%)} = \frac{\text{Moles of hydrogen produced}}{2 \times \text{mole of } CH_{4 \text{ in feed}}} \times 100\% \quad (2)$$

where the volume of  $CH_4$  at the reactor inlet and outlet are represented by  $CH_{4in}$ , and  $CH_{4out}$ , accordingly.

The physicochemical characteristics of fresh catalysts and those tested in methane decomposition were studied by X-ray phase analysis (XRD), Brunauer-Emmett-Taylor (BET), temperature-programmed hydrogen reduction (TPR- $H_2$ ), and Raman spectroscopy.

### 3. Results and discussion

The results of comparative activity in the methane decomposition of  $Fe_2O_3$ -NiO/ $Al_2O_3$  catalyst synthesized by capillary impregnation ( $Fe_2O_3$ -NiO/ $Al_2O_3$ (CI)) and solution combustion ( $Fe_2O_3$ -NiO/ $Al_2O_3$ (SC)) are shown in Fig. 2.

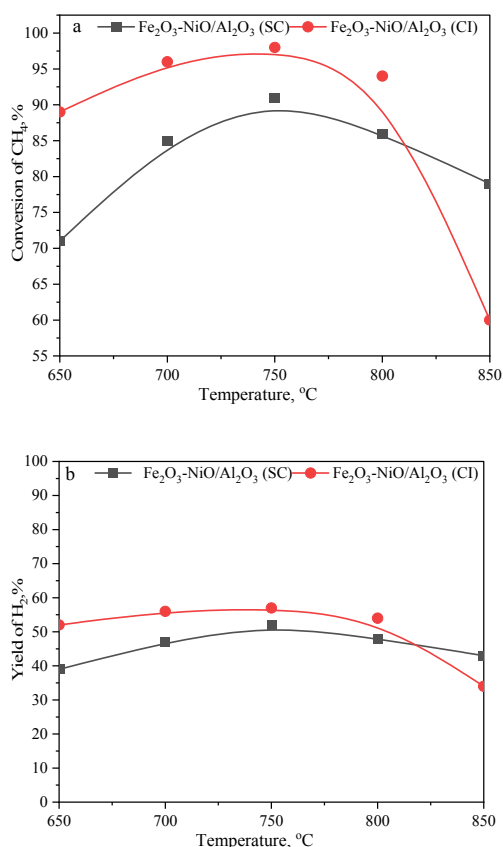


Fig. 2. Effect of reaction temperature on activity of  $Fe_2O_3$ -NiO/ $Al_2O_3$  (CI) and  $Fe_2O_3$ -NiO/ $Al_2O_3$  (SC) catalysts in decomposition of methane: conversion of methane (a), yield of hydrogen (b).

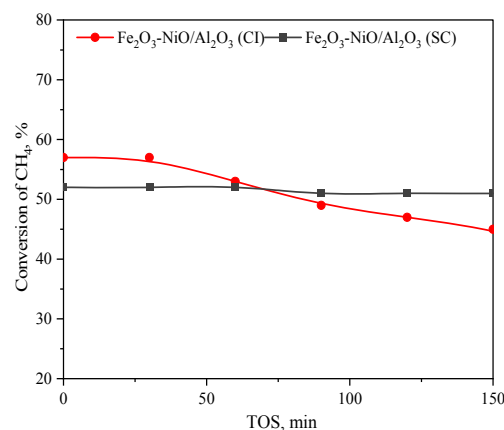


Fig. 3. Stability performance of catalysts in terms of  $CH_4$  conversion at 750  $^{\circ}C$ .

Investigation of the activity of catalysts in the temperature range of 650–850  $^{\circ}C$  showed that on the  $Fe_2O_3$ -NiO/ $Al_2O_3$  (CI), the methane conversion and hydrogen yield increase in the temperature range of 650–800  $^{\circ}C$  from 90 to 94%, from 52 to 54%, respectively, passing through a maximum at 750  $^{\circ}C$ . A further increase in the reaction temperature to 850  $^{\circ}C$  leads to a decrease in the activity of the catalyst. A similar character is also observed for  $Fe_2O_3$ -NiO/ $Al_2O_3$  (SC), but with lower catalytic activity. The highest methane conversion of 98% and hydrogen yield of 57% at a reaction temperature of 750  $^{\circ}C$  are observed for the  $Fe_2O_3$ -NiO/ $Al_2O_3$  (CI) catalyst. However, for the catalyst  $Fe_2O_3$ -NiO/ $Al_2O_3$  (CI) at 850  $^{\circ}C$  there is a sharp decrease in activity compared to  $Fe_2O_3$ -NiO/ $Al_2O_3$  (SC).

Catalysts  $Fe_2O_3$ -NiO/ $Al_2O_3$  (CI) and  $Fe_2O_3$ -NiO/ $Al_2O_3$  (SC) were tested at a reaction temperature of 750  $^{\circ}C$  in methane decomposition for 150 min (Fig. 3). The conversion profiles showed that  $Fe_2O_3$ -NiO/ $Al_2O_3$  (CI) had an initial conversion of 57%, which decreased starting at 60 min and reached 47% at 150 min. Compared to  $Fe_2O_3$ -NiO/ $Al_2O_3$  (CI), the  $Fe_2O_3$ -NiO/ $Al_2O_3$  (SC) catalyst had a lower initial conversion of 52% however, the catalyst did not decrease its activity within 150 min.

The results of BET showed that the specific surface area of the catalysts did not differ much from each other. The specific surface of the catalyst prepared by capillary impregnation of  $Fe_2O_3$ -NiO/ $Al_2O_3$  (CI) is 89.7  $m^2/g$ , while the catalyst prepared by the combustion solution method  $Fe_2O_3$ -NiO/ $Al_2O_3$  (SC) is 94.6  $m^2/g$ .

X-Ray diffractions patterns of fresh catalysts are shown in Fig. 4.

The diffraction peaks at  $2\theta = 30.4, 37.4, 45.3^{\circ}$  are mainly related to  $Fe_2O_3$  (JCPDS, no. 39-1346).

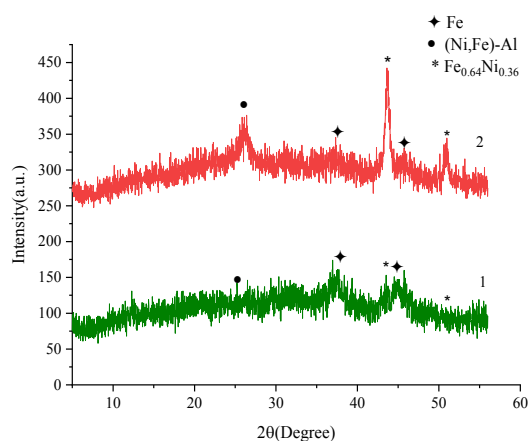


Fig. 4. XRD patterns of fresh catalysts: 1 – Fe<sub>2</sub>O<sub>3</sub>-NiO/Al<sub>2</sub>O<sub>3</sub> (CI); 2 – Fe<sub>2</sub>O<sub>3</sub>-NiO/Al<sub>2</sub>O<sub>3</sub> (SC).

Characteristic peaks of the FeNi alloy (JCPDS, no. 38-0419) can be observed at  $2\theta = 44.2, 51.5$  on the X-ray diffraction patterns of the catalysts, for the Fe<sub>2</sub>O<sub>3</sub>-NiO/Al<sub>2</sub>O<sub>3</sub> (SC) catalyst with greater intensity. The absence of the peaks from the crystal lattice of the NiO suggests that the oxide in the synthesized catalysts is presented in the form of nanoparticles with sizes much smaller than the X-ray diffraction sensitivity threshold for the coherent scattering area size ( $<100 \text{ \AA}$ ).

The reduction characteristics of Fe<sub>2</sub>O<sub>3</sub>-NiO/Al<sub>2</sub>O<sub>3</sub> (CI), Fe<sub>2</sub>O<sub>3</sub>-NiO/Al<sub>2</sub>O<sub>3</sub> (SC), and monometallic Fe<sub>2</sub>O<sub>3</sub>/Al<sub>2</sub>O<sub>3</sub> (CI), NiO/Al<sub>2</sub>O<sub>3</sub> (CI) catalysts were studied by the TPR-H<sub>2</sub> method. The results are shown in Fig. 5.

The TPR profile of Ni/γ-Al<sub>2</sub>O<sub>3</sub> (CI) shows four peaks with temperature maxima at  $T^1_{\max} = 487 \text{ }^\circ\text{C}$ , (hydrogen amount  $A = 13 \text{ } \mu\text{mol/gKt}$ ),  $T^2_{\max} = 652 \text{ }^\circ\text{C}$ , ( $A = 369 \text{ } \mu\text{mol/gKt}$ ),  $T^3_{\max} = 740 \text{ }^\circ\text{C}$ , ( $A = 44 \text{ } \mu\text{mol/gKt}$ ) and  $T^4_{\max} = 780 \text{ }^\circ\text{C}$ , ( $A = 135 \text{ } \mu\text{mol/gKt}$ ). The peak at  $T^1_{\max}$  refers to the reduction of nickel cations in the composition of NiO particles not bound to the support [15]. Peaks  $T^2_{\max}$  and

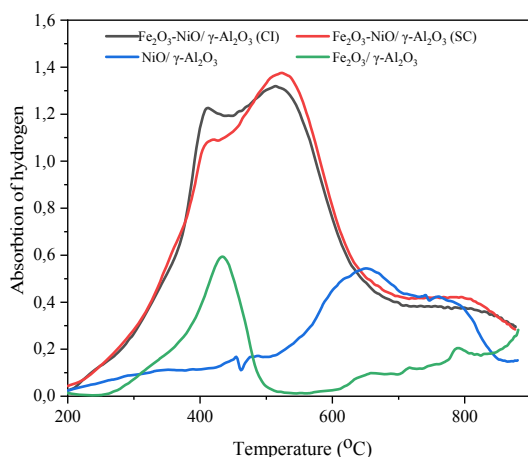


Fig. 5. TPR profile of catalysts.

$T^3_{\max}$  refer to the reduction of nickel oxide particles characterized by “weak” and “strong” metal-carrier interactions [16]. The peak with a maximum at  $T^4_{\max} = 780 \text{ }^\circ\text{C}$  is associated with the presence of dispersed spinel-like forms of NiAl<sub>2</sub>O<sub>4</sub> in the sample [17].

The TPR profile of Fe/Al<sub>2</sub>O<sub>3</sub> (CI) shows an intense peak with a temperature maximum at  $T^1_{\max} = 434 \text{ }^\circ\text{C}$ , ( $A = 342 \text{ } \mu\text{mol/gKt}$ ). In addition, there are low-intensity peaks at  $T^2_{\max} = 660 \text{ }^\circ\text{C}$  ( $A = 10 \text{ } \mu\text{mol/gKt}$ ),  $T^3_{\max} = 717 \text{ }^\circ\text{C}$  ( $A = 2 \text{ } \mu\text{mol/gKt}$ ) and  $T^4_{\max} = 790 \text{ }^\circ\text{C}$  ( $A = 9 \text{ } \mu\text{mol/gKt}$ ). The peak at  $T^1_{\max} = 434 \text{ }^\circ\text{C}$  is associated with the reduction of Fe<sub>2</sub>O<sub>3</sub> to Fe<sub>3</sub>O<sub>4</sub> [18]. Peaks in the region of  $650\text{--}720 \text{ }^\circ\text{C}$  can be attributed to the reduction of oxide Fe<sub>3</sub>O<sub>4</sub> to FeO. The presence of several peaks may indicate the interaction of the metal-carrier, characterized by different strengths. The peak at  $T^4_{\max} = 790 \text{ }^\circ\text{C}$  can be associated with the presence of the hard-to-recover FeAl<sub>2</sub>O<sub>4</sub> phase.

The TPR profiles of bimetallic catalysts differ from those of monometallic ones. The profiles of Fe<sub>2</sub>O<sub>3</sub>-NiO/γ-Al<sub>2</sub>O<sub>3</sub> (CI) and Fe<sub>2</sub>O<sub>3</sub>-NiO/γ-Al<sub>2</sub>O<sub>3</sub> (SC) catalysts are of the same character, there are three peaks with different intensities. The TPR profile of Fe<sub>2</sub>O<sub>3</sub>-NiO/γ-Al<sub>2</sub>O<sub>3</sub> (CI) has peaks with maxima  $T^1_{\max} = 413 \text{ }^\circ\text{C}$  ( $A = 668 \text{ } \mu\text{mol/gKt}$ ),  $T^2_{\max} = 514 \text{ }^\circ\text{C}$  ( $A = 1162 \text{ } \mu\text{mol/gKt}$ ) and  $T^3_{\max} = 710 \text{ }^\circ\text{C}$  ( $A = 127 \text{ } \mu\text{mol/gKt}$ ). The TPR profile of Fe<sub>2</sub>O<sub>3</sub>-NiO/γ-Al<sub>2</sub>O<sub>3</sub> (SC) has three peaks too with maxima  $T^1_{\max} = 415 \text{ }^\circ\text{C}$  ( $A = 504 \text{ } \mu\text{mol/gKt}$ ),  $T^2_{\max} = 526 \text{ }^\circ\text{C}$  ( $A = 1326 \text{ } \mu\text{mol/gKt}$ ) and  $T^3_{\max} = 795 \text{ }^\circ\text{C}$  ( $A = 164 \text{ } \mu\text{mol/gKt}$ ).

The first peak can be attributed to the reduction of Fe<sub>2</sub>O<sub>3</sub> unbound to the support. Compared to a monometallic catalyst, on bimetallic catalysts the temperature maximum related to the reduction of Fe<sub>2</sub>O<sub>3</sub> shifts to the low-temperature region from 434 to 413–415 °C. Compared to Fe<sub>2</sub>O<sub>3</sub>-NiO/γ-Al<sub>2</sub>O<sub>3</sub> (SC) on the TPR profile of the Fe<sub>2</sub>O<sub>3</sub>-NiO/γ-Al<sub>2</sub>O<sub>3</sub> (CI) catalyst, the intensity of the peak related to the reduction of Fe<sub>2</sub>O<sub>3</sub> is higher, which indicates a high content of Fe<sub>2</sub>O<sub>3</sub> unbound to the support. A new peak appears on the TPR profile of bimetallic catalysts with maxima at 514 and 526 °C, which are not observed on the TPR profile of monometallic catalysts. The presence of this peak may indicate the formation of the FeNi alloy, these data are confirmed by the XRD results (Fig. 4). The intensity of this peak on the Fe<sub>2</sub>O<sub>3</sub>-NiO/γ-Al<sub>2</sub>O<sub>3</sub> (SC) catalyst is higher compared to Fe<sub>2</sub>O<sub>3</sub>-NiO/γ-Al<sub>2</sub>O<sub>3</sub> (CI), which may indicate a larger amount of this phase on the Fe<sub>2</sub>O<sub>3</sub>-NiO/γ-Al<sub>2</sub>O<sub>3</sub> (SC) compared

with  $\text{Fe}_2\text{O}_3\text{-NiO}/\gamma\text{-Al}_2\text{O}_3$  (CI). The peak at  $T_{\text{max}}^3 = 795\text{ }^\circ\text{C}$  ( $A = 164\text{ }\mu\text{mol/g}$ ) can be attributed to the reduction of aluminates, possibly  $\text{FeAl}_2\text{O}_4$ , since the reduction of  $\text{NiAl}_2\text{O}_4$  is observed at a lower temperature ( $T_{\text{max}}^4 = 780\text{ }^\circ\text{C}$ ).

Compared to  $\text{Fe}_2\text{O}_3\text{-NiO}/\gamma\text{-Al}_2\text{O}_3$  (CI) on the  $\text{Fe}_2\text{O}_3\text{-NiO}/\gamma\text{-Al}_2\text{O}_3$  (SC) catalyst, the intensity of the peak related to the reduction of aluminates is higher, which indicates a higher content of aluminates.

Therefore, the most stable activity in the decomposition of methane of the catalyst  $\text{Fe}_2\text{O}_3\text{-NiO}/\gamma\text{-Al}_2\text{O}_3$  (SC) in comparison with  $\text{Fe}_2\text{O}_3\text{-NiO}/\gamma\text{-Al}_2\text{O}_3$  (CI) is possibly associated with a high content of  $\text{NiAl}_2\text{O}_4$  or  $\text{FeAl}_2\text{O}_4$  solid solutions. It is known [19] that the reduction of  $\text{NiAl}_2\text{O}_4$  spinel produces finely dispersed nickel (5–20 nm) stabilized in an  $\text{Al}_2\text{O}_3$  matrix, which is highly active in the methane dissociation reaction. At high temperatures, spinel will be reduced to finely dispersed nickel by atomic hydrogen, which is formed during the dissociation of methane. Therefore, this property provides good catalytic activity at high temperatures as well as caking resistance.

The carbon structure was analyzed using Raman spectroscopy. Figure 6 shows the spectra of the catalysts tested in the decomposition of methane at  $750\text{ }^\circ\text{C}$  for 150 min.

Band G, located at a frequency of  $1572\text{ cm}^{-1}$ , refers to the vibration of graphite in the C-C plane. The peak at  $1357\text{ cm}^{-1}$  is called the D band derived from amorphous carbon or imperfect graphite. It is known [20] that the D band on the Raman spectrum is usually very weak in graphite and high quality graphene. The intensity of the D band is directly proportional to the level of defects in the sample. The results of Raman spectroscopy show a high intensity of the bands in the range of  $500\text{--}1000\text{ cm}^{-1}$  and the D band in the  $\text{Fe}_2\text{O}_3\text{-NiO}/\gamma\text{-Al}_2\text{O}_3$  (SC) spectra, which indicates the defectiveness of the deposited carbon. Therefore, in the areas of  $\text{Fe}_2\text{O}_3\text{-NiO}/\gamma\text{-Al}_2\text{O}_3$  (SC) not covered with carbon, methane will decompose until all catalyst particles are completely covered with carbon.

The relative intensity ratio in the form of  $I_{\text{D}}/I_{\text{G}}$

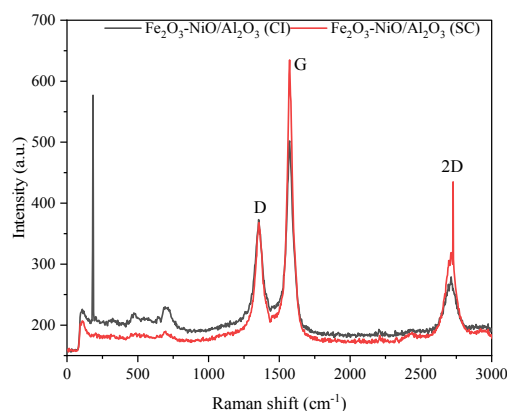


Fig. 6. Raman spectra of  $\text{Fe}_2\text{O}_3\text{-NiO}/\gamma\text{-Al}_2\text{O}_3$  (SC) and  $\text{Fe}_2\text{O}_3\text{-NiO}/\gamma\text{-Al}_2\text{O}_3$  (CI) after the methane decomposition.

is used to quantify the degree of graphitization of deposited carbon [21]. Namely, as the degree of graphitization increases, the  $I_{\text{D}}/I_{\text{G}}$  ratio decreases. The  $I_{\text{D}}$ ,  $I_{\text{G}}$ ,  $I_{2\text{D}}$  intensities and calculated ratios are shown in Table. The  $I_{\text{D}}/I_{\text{G}}$  value of deposited carbon on  $\text{Fe}_2\text{O}_3\text{-NiO}$  (CI) is 0.75, on  $\text{Fe}_2\text{O}_3\text{-NiO}$  (SC) is 0.58. Higher  $I_{\text{D}}/I_{\text{G}}$  values indicate a lower degree of graphitization of deposited carbon, which is consistent with the results. The 2D band ( $\sim 2700\text{ cm}^{-1}$ ) is characteristic of structures with several and several layers of graphene and graphite. Similar spectra are found in the literature for multilayer graphene and graphite [22, 23]. It is known [24] that the ratio between the intensities of the 2D peak ( $I_{2\text{D}}$ ) and the G peak ( $I_{\text{G}}$ ) gives an estimate of the number of layers. The  $I_{2\text{D}}/I_{\text{G}}$  value of deposited carbon on  $\text{Fe}_2\text{O}_3\text{-NiO}/\gamma\text{-Al}_2\text{O}_3$  (CI) is 0.56, on  $\text{Fe}_2\text{O}_3\text{-NiO}/\gamma\text{-Al}_2\text{O}_3$  (SC) is 0.50. According to [25], the ratio  $I_{2\text{D}}/I_{\text{G}} = 0.56$  indicates 4 or 5 graphene layers,  $I_{2\text{D}}/I_{\text{G}} = 0.50$  indicates 6 or 7 graphene layers.

From the results of Raman spectroscopy, it follows that after testing the catalysts  $\text{Fe}_2\text{O}_3\text{-NiO}/\gamma\text{-Al}_2\text{O}_3$  (CI) and  $\text{Fe}_2\text{O}_3\text{-NiO}/\gamma\text{-Al}_2\text{O}_3$  (SC) in the decomposition of methane at  $750\text{ }^\circ\text{C}$ , deposition of graphene-like carbon is observed on the catalysts. On the  $\text{Fe}_2\text{O}_3\text{-NiO}/\gamma\text{-Al}_2\text{O}_3$  (CI) catalyst, 4–5 layer graphene is formed on  $\text{Fe}_2\text{O}_3\text{-NiO}/\gamma\text{-Al}_2\text{O}_3$  (SC)-6–7 layer graphene.

**Table**  
Raman intensities for  $I_{\text{D}}$ ,  $I_{\text{G}}$ ,  $I_{2\text{D}}$ ,  $I_{\text{D}}/I_{\text{G}}$  and  $I_{2\text{D}}/I_{\text{G}}$

Sample	Intensity (a.u)			$I_{\text{D}}/I_{\text{G}}$	$I_{2\text{D}}/I_{\text{G}}$	Remarks
	$I_{\text{D}}$	$I_{\text{G}}$	$I_{2\text{D}}$			
$\text{Fe}_2\text{O}_3\text{-NiO}/\gamma\text{-Al}_2\text{O}_3$ (CI)	369	494	279	0.75	0.56	4 or 5 layers of graphene
$\text{Fe}_2\text{O}_3\text{-NiO}/\gamma\text{-Al}_2\text{O}_3$ (SC)	368	635	319	0.58	0.50	6 or 7 layers of graphene

#### 4. Conclusions

In order to develop an efficient catalyst for hydrogen production by methane decomposition, the effect of synthesis methods, such as capillary impregnation and solution combustion, on the activity of the Fe<sub>2</sub>O<sub>3</sub>-NiO/γ-Al<sub>2</sub>O<sub>3</sub> catalyst was studied. The results of the catalytic efficiency tests showed that the activity and stability of the catalyst can be controlled by preparation techniques. According to the results of the studies, the synthesis of the Fe<sub>2</sub>O<sub>3</sub>-NiO/γ-Al<sub>2</sub>O<sub>3</sub> catalyst by capillary impregnation increases the proportion of iron oxide not bound to the support, which leads to an increase in its activity in the decomposition of methane at relatively low temperatures. The preparation of Fe<sub>2</sub>O<sub>3</sub>-NiO/γ-Al<sub>2</sub>O<sub>3</sub> by the solution combustion method leads to the formation of FeNi and FeAl<sub>2</sub>O<sub>4</sub>, which provided good catalytic activity at high temperatures due to the high dispersion of active metals.

The Fe<sub>2</sub>O<sub>3</sub>-NiO/γ-Al<sub>2</sub>O<sub>3</sub> catalyst synthesized by the solution combustion method demonstrated good activity with a hydrogen yield of 52% within 150 min of the reaction without any deactivation. According to the results of Raman spectroscopy, graphene-like carbon was obtained on the surface of the catalysts. On the catalyst of Fe<sub>2</sub>O<sub>3</sub>-NiO/γ-Al<sub>2</sub>O<sub>3</sub> (CI) synthesized by capillary impregnation, 4–5 layer graphene on Fe<sub>2</sub>O<sub>3</sub>-NiO/γ-Al<sub>2</sub>O<sub>3</sub> (SC)-6–7 layer graphene is formed.

#### Acknowledgments

This work was supported by a grant from the Ministry of Education and Science of the Republic of Kazakhstan № AP08855564 “Obtaining hydrogen and nanocarbon from natural gas – methane”.

#### References

- [1]. D.D.T. Ferraren-De Cagalitan, M.L.S. Abundo, *Renew. Sust. Energy Rev.* 151 (2021) 111413. DOI: [10.1016/j.rser.2021.111413](https://doi.org/10.1016/j.rser.2021.111413)
- [2]. G.E. Ergazieva, N. Makayeva, Z. Shaimerden, S.O. Soloviev, M. Telbayeva, E. Akkazin, F. Ahmetova, *Bull. Chem. React. Eng. Catal.* 17 (2022). DOI: [10.9767/bcrec.17.1.12174.1-12](https://doi.org/10.9767/bcrec.17.1.12174.1-12)
- [3]. H.F. Abbas, W.M.A. Wan Daud, *Int. J. Hydrogen Energy* 35 (2010) 1160–1190. DOI: [10.1016/j.ijhydene.2009.11.036](https://doi.org/10.1016/j.ijhydene.2009.11.036)
- [4]. Z. Fan, W. Weng, J. Zhou, D. Gu, W. Xiao, *J. Energy Chem.* 58 (2021) 415–430. DOI: [10.1016/j.jechem.2020.10.049](https://doi.org/10.1016/j.jechem.2020.10.049)
- [5]. K. Murata, M. Inaba, M. Saito, I. Takahara, N. Mimura, *J. Jpn. Petrol. Inst.* 46 (2003). DOI: [10.1627/JPI.46.196](https://doi.org/10.1627/JPI.46.196)
- [6]. A.S. Al-Fatesh, A.A. Ibrahim, A.M. AlSharekh, F.S. Alqahtani, S.O. Kasim, A.H. Fakeeha, *Egypt. J. Pet.* 27 (2018) 1221–1225. DOI: [10.1016/J.EJPE.2018.05.004](https://doi.org/10.1016/J.EJPE.2018.05.004)
- [7]. J. Chen, X. Zhou, L. Cao, Y. Li, *Stud. Surf. Sci. Catal.* 147 (2004) 73–78. DOI: [10.1016/S0167-2991\(04\)80030-2](https://doi.org/10.1016/S0167-2991(04)80030-2)
- [8]. J.L. Pinilla, R. Utrilla, R.K. Karn, I. Suelves, M.J. Lazaro, R. Moliner, A.B. Garcia, J.N. Rouzaud, *Int. J. Hydrogen Energy* 36 (2011) 7832–7843. DOI: [10.1016/j.ijhydene.2011.01.184](https://doi.org/10.1016/j.ijhydene.2011.01.184)
- [9]. L.B. Avdeeva, T.V. Reshетенko, Z.R. Ismagilov, V.A. Likholobov, *Appl. Catal. A: Gen.* 228 (2002) 53–63. DOI: [10.1016/S0926-860X\(01\)00959-0](https://doi.org/10.1016/S0926-860X(01)00959-0)
- [10]. D. Torres, J.L. Pinilla, M.J. Lazaro, R. Moliner, I. Suelves, *Int. J. Hydrogen Energy* 39 (2014) 3698–3709. DOI: [10.1016/J.IJHYDENE.2013.12.127](https://doi.org/10.1016/J.IJHYDENE.2013.12.127)
- [11]. M. Pudukudy, Z. Yaakob, Z.S. Akmal, *Appl. Surf. Sci.* 330 (2015) 4185–430. DOI: [10.1016/J.APSUSC.2015.01.032](https://doi.org/10.1016/J.APSUSC.2015.01.032)
- [12]. G. Yergaziyeva, N. Makayeva, A. Abdisattar, M. Yeleuov, S. Soloviev, M. Anissova, A. Taurbekov, K. Dossumov, E. Akkazin, C. Daulbayev, *Chem. Pap.* (2022). DOI: [10.1007/s11696-022-02420-9](https://doi.org/10.1007/s11696-022-02420-9)
- [13]. K. Dossumov, G.E. Ergazieva, B.T. Ermagambet, M.M. Mambetova, Z. Kassenova, *Russ. J. Phys. Chem.* 94 (2020) 880–882. DOI: [10.1134/S0036024420040020](https://doi.org/10.1134/S0036024420040020)
- [14]. G. Yergaziyeva, K. Dossumov, M. Mambetova, P.Y. Strizhak, H. Kurokawa, B. Baizhomartov, *Chem. Eng. Technol.* 44 (2021) 1890–1899. DOI: [10.1002/ceat.202100112](https://doi.org/10.1002/ceat.202100112)
- [15]. C.H. Campos, P. Osorio-Vargas, N. Flores-González, J.L.G. Fierro, P. Reyes, *Catal. Lett.* 146 (2016) 433–441. DOI: [10.1007/s10562-015-1649-6](https://doi.org/10.1007/s10562-015-1649-6)
- [16]. S. Pengpanich, V. Meeyoo, T. Rirksomboon, *Catal. Today* 93–95 (2004) 95–105. DOI: [10.1016/j.cattod.2004.06.079](https://doi.org/10.1016/j.cattod.2004.06.079)
- [17]. A. Horváth, M. Németh, A. Beck, B. Maróti, G. Sáfrán, G. Pantaleo, L.F. Liotta, A.M. Venezia, V. La Parola, *Appl. Catal. A: Gen.* 621 (2021) 118174. DOI: [10.1016/j.apcata.2021.118174](https://doi.org/10.1016/j.apcata.2021.118174)
- [18]. J. Zhang, L. Jin, Y. Li, H. Hu, *Int. J. Hydrogen Energy* 38 (2013) 3937–3947. DOI: [10.1016/j.ijhydene.2013.01.105](https://doi.org/10.1016/j.ijhydene.2013.01.105)
- [19]. S.O. Soloviev, I.V. Gubareni, S.M. Orlyk, *Theor. Exp. Chem.* 54 (2018) 293–315. DOI: [10.1007/s11237-018-9575-5](https://doi.org/10.1007/s11237-018-9575-5)
- [20]. H. Nishii, D. Miyamoto, Y. Umeda, H. Hamaguchi, M. Suzuki, T. Tanimoto, *Appl.*

- Surf. Sci.* 473 (2019) 291–297. DOI: [10.1016/j.apsusc.2018.12.073](https://doi.org/10.1016/j.apsusc.2018.12.073)
- [21]. Y. Yu, F. Fu, L. Shang, Y. Cheng, Z. Gu, Y. Zhao, *Adv. Mater.* 29 (2017) 1605765. DOI: [10.1002/adma.201605765](https://doi.org/10.1002/adma.201605765)
- [22]. A. Gupta, G. Chen, P. Joshi, S. Tadigadapa, P.C. Eklund, *Nano Lett.* 6 (2006) 2667–2673. DOI: [10.1021/nl061420a53](https://doi.org/10.1021/nl061420a53)
- [23]. E. Sallah, W. Al-Shatty, C. Pleydell-Pearce, A.J. London, C. Smith, *Carbon Trends* 8 (2022) 100174. DOI: [10.1016/j.cartre.2022.100174](https://doi.org/10.1016/j.cartre.2022.100174)
- [24]. N.K. Memon, S.D. Tse, J.F. Al-Sharab, H. Yamaguchi, A.-M. Goncalves, B.H. Kear, Y. Jaluria, E.Y. Andrei, M. Chhowalla, *Carbon* 49 (2011) 5064–5070. DOI: [10.1016/j.carbon.2011.07.024](https://doi.org/10.1016/j.carbon.2011.07.024)
- [25]. U. Kalsoom, M.S. Rafique, S. Shahzadi, K. Fatima, N.R. Shaheen, *Mater. Sci.-Poland* 35 (2018) 687–693. DOI: [10.1515/msp-2017-0099](https://doi.org/10.1515/msp-2017-0099)
- [26]. M. Yeleuov, C. Seidl, T. Temirgaliyeva, A. Taurbekov, N. Prikhodko, B. Lesbayev, F. Sultanov, C. Daulbayev, S. Kumekov, *Energies* 13 (2020) 4943. DOI: [10.3390/en13184943](https://doi.org/10.3390/en13184943)